Desalination and Water Treatment
www.deswater.com

doi: 10.5004/dwt.2023.30195

316 (2023) 290–298
December

Applications of the synthesized iron nanoparticles in the degradation of p-nitrophenol

Zeyan Wu†, Quanju Yang†, Minghua Li, Ye Zhang*, Kezhen Qi*

College of Pharmacy, Dali University, Dali 671000, China, emails: dlzhangye@126.com (Y. Zhang), qkzh2003@aliyun.com (K. Qi)

Received 21 September 2023; Accepted 3 December 2023

ABSTRACT

p-nitrophenol (4-NP) is a common raw material in the industrial production of many valuable substances. With the rapid development of chemical industry, the production of 4-NP has increased substantially. However, due to its characteristic toxicity, p-nitrophenol inevitably causes pollution to the environment during its synthesis and usage. In this paper, sodium borohydride ($NaBH_4$) and ferric chloride ($FeCl_3·6H_2O$) were used as raw materials to prepare iron nanoparticles by liquid phase reduction technique, and their performance in 4-NP pollutant degradation was investigated. The experimental results showed that the iron nanoparticles presented excellent degradation performance for 4-NP. When the concentration of 4-NP was 15 mg/L, only 0.25 g/L of iron nanoparticles degraded more than 74% of 4-NP in 1 h.

Keywords: p-nitrophenol; Iron nanoparticles; Cu^{2+} interfering ions; Degradation; Reaction pathway

1. Introduction

In the past few decades, the excessive emission of CO_2 has caused greenhouse effect responsible for global warming, rise in global temperature, energy crisis, and serious pollution of the environment and water resources. Environmental pollution is increasingly becoming a global problem that may cause greater harm to nature and human health, ecosystems, and sustainable development of society, so there is an urgent need to remove harmful pollutants from ecosystems [1–6]. The main causes of environmental pollution have been the printing and dyeing industry, the textile industry, the pharmaceutical industry, municipal effluents, hospitals, and slaughterhouse wastes. Among these, bio-toxic pesticides such as dichlorvos [7], aromatic hydrocarbon pollutants [8], phenols and halophenols [9], insecticides, herbicides, and other harmful organic pollutants are all frequently detected in various water bodies such as rivers, lakes, surface water, and underground environments. At present, adsorption and degradation are frequently used to deal with harmful organic pollutants and ultimately achieve environmental remediation. Many authors have employed adsorption [10–14], photocatalysis [15–17], sonocatalysis [18], etc techniques to remove harmful pollutants. p-nitrophenol (4-NP) is one of the most common aromatic organic pollutants and mainly comes from pharmaceutical, plastic, dye, and other industries, in which hydroxyl and nitro groups are directly linked with the benzene ring. It is soluble in water with enormous toxicity and is extremely harmful to human body, such as confusion, skin and eye irritation, loss of consciousness, and even potential carcinoma. It is a biologically active, chemically stable, bio-accumulative, persistent, and highly toxic pollutant that is not easily degraded under ordinary conditions [19,20]. It is particularly difficult to eradicate through natural biodegradation [21]. In addition, 4-NP is a protoplasmic poison that can enter the blood circulation through human epidermal cells, and if exposed to it for a long time even in low concentrations, it is very likely to lead to abnormal hemoglobin, liver, and kidney damage, and carcinogenic and mutagenic [22,23] lesions. Also, 4-NP discharged into the water system can cause the death of aquatic organisms.

* Corresponding authors.
† These authors contributed equally to this work.

Since it poses a great threat to human development and ecosystem stability, it is classified as a priority pollutant by the U.S. Environmental Protection Agency (EPA), specifying a maximum concentration of 20 mg/L in industrial wastewater. Keeping in view its hazardous effects, there is an urgent need to find cost-effective methods and materials to remove 4-NP from wastewater. However, it is one of the major challenges faced by environmental engineers today. Therefore, this important issue has presently inspired a great deal of research for the removal of hazardous substances for environmental remediation [24].

Although, adsorption [25], advanced oxidation and reduction process [26–29], photo/electrocatalytic removal [30], and biochemical methods [31] etc. have been employed to eliminate p-aminophenol including, but the disadvantages of these methods are sophisticated, expensive equipment's and high energy consumption. Therefore, it is particularly important to seek an efficient and environmentally friendly technology to remove p-nitrophenol. Among them, direct reduction method can reduce 4-NP to p-aminophenol, its application as photographic developing agent, corrosion inhibitor, dyeing agent, and active intermediate for the synthesis of paracetamol, phenacetin drugs and its toxicity is reduced by about 500 times [32,33]. Fe nanoparticles as a potential alternative source of Fe^{2+} have been successfully used to activate hydrogen peroxide to degrade various pollutants [34]. Fe NP can be coupled with other elements, like noble metals (e.g., Pd, Ag, Cu, Ni, etc.), also in nanoparticle form, or carbonaceous material [35]. Studies have shown that Fe NP has significant adsorption and degradation efficiency for several heavy metals and different organic pollutants [36–39]. In recent years, research on nanomaterials has increased by many folds, and therefore investigation of the preparation methods (development of new reactions/reaction conditions), microstructure (adjustment of topography and surface defects), and reaction dynamics has emerged as breakthroughs in nanotechnology [40–43]. Zhu et al. [44] prepared Fe/Ni bimetallic nanoparticles by the liquid phase reduction method for the treatment of hexavalent chromium ions in soil leachate, and the removal rate for hexavalent chromium could reach 99.8% under the condition of pH = 5 at 30°C. Kim et al. [45] used $Na_2S_2O_4$ and $NaBH_4$ to prepare sulfide-covered Fe NPs. Under synthetic and real groundwater conditions, the synthesized FeS-covered Fe NPs showed great advantages in the removal reaction of trichloroethylene. Dutta et al. [46] prepared Fe NPs with better stability by improving the preparation method, which was used to remove azo dyes in textile wastewater, and the removal efficiency was good, up to 97%. At present, the synthesis method of Fe NPs can be roughly divided into physical or chemical methods. The required Fe NP is prepared by chemical methods. Among them, the liquid phase reduction method uses chemical substances with strong reducing properties such as KBH_4, $NaBH_4$, or organic metal reduction agents in the liquid phase system to reduce Fe^{2+} and Fe^{3+} to form nanometer iron particles. This synthesis route is not complicated but is fast response, low cost, and simple operation, and the required equipment and reaction conditions are easy to implement, so that which is one of the most common preparation methods for Fe NPs.

In this study, iron nanoparticles were prepared by liquid phase reduction method. The highlight of this work is that 74% of 15 mol/L p-nitrophenol was degraded by Fe within 60 min without external conditions such as light source. When doped with low concentration of Cu^{2+}, the degradation efficiency of 4-NP reaches 84%, which has better degradation effect than other degradation technologies. The aim of this study is to provide a new way to remove dyes and effectively carry out environmental remediation.

2. Experimental part

2.1. Reagent

All the reagents used in this study were analytical grade and used without further purification. p-nitrophenol (4-NP) was purchased from Kamishor Biotechnology Co., Ltd., (China). Sodium borohydride, $FeCl_3{\cdot}6H_2O$, $CuSO_4{\cdot}5H_2O$, $MnSO_4{\cdot}H_2O$ and $ZnSO_4{\cdot}7H_2O$ were purchased from Tianjin Kemiou Chemical Reagent Co., Ltd., (China). Absolute ethanol (C_2H_5OH) was purchased from Yunnan Yanglin Industrial Development Zone Shandian Pharmaceutical Co., Ltd., (China). Nickel nitrate hexahydrate ($Ni(NO_3)_2{\cdot}6H_2O$) was purchased from Chengdu Chemical Reagent Factory. Deionized water (conductivity 18.25 μS/cm) was homemade in the laboratory.

2.2. Preparation of Fe NPs

In this work, the liquid phase reduction method was used to prepare Fe NPs. Accurately weighed 6.0 g $NaBH_4$ powder was dissolved in 400 mL distilled water. 3.0 g solid $FeCl_3{\cdot}6H_2O$ was completely dissolved in 1,000 mL distilled water, and $NaBH_4$ solution was added to the $FeCl_3$ solution dropwise with a rubber tip dropper under stirring for 10 min. The mixture was placed in a cool place protected from light and aged for 2.5 h. After aging, the supernatant was removed, the remaining mixture was filtered in a Brinell funnel and washed with 100 mL deionized water and 100 mL C_2H_5OH. The black residue was put in a small beaker and dried under an infrared lamp for 2.5 h under argon gas. During that time, the solid was mashed every 30–60 min. Finally, the cooled product was obtained as Fe NPs.

2.3. Preparation of experimental solution

Accurately weighed 75 mg solid 4-NP was dissolved in deionized water and diluted with more deionized water in a 250 mL volumetric flask under shaking. The obtained stock solution of 4-NP had a concentration of 300 mg/L and was placed in a cool and dry place. From the stock solution, a 500 mL 4-NP solution of 15 mg/L was prepared through the dilution technique with deionized water for the degradation experiment. Other solutions of 4-NP with different concentrations were also prepared.

2.4. Characterization

Bruker X-ray diffraction (Germany) examined the crystal structure of the prepared sample. X-ray photoelectron spectroscopy (XPS) studies were performed on the samples using Escalab 250Xi rays produced by Thermo Fisher Scientific

(America). High-resolution transmission electron microscopy and scanning electron microscopy (SEM) images were obtained using the Talos F200X (America) and JSM-7500F (Japan).

2.5. Setting of experimental systems

4-NP solutions with different concentrations were prepared and their absorbances at the maximum absorption wavelength of 317 nm were measured with a dual-beam UV-Vis spectrophotometer. When the concentration of 4-NP solution was 15 mg/L, the degradation volume was 200 mL, and the amount of Fe NPs was 50 mg. After 4 h, the absorbance at 317 nm was 1.008, which conformed the precision range (absorbance ≤ 1.2) of a dual-beam UV-Vis spectrophotometer. The effect of the different time of Fe NPs on the degradation of (15 mg/L) 4-NP solution was investigated and the degradation rate of 4-NP with nano-iron was measured using the equation: $D(\%) = C_o - C/C_o \times 100$, where D is the degradation rate of 4-NP, C_o is the initial concentration and C is the concentration after degradation for a certain period.

2.6. Effects of oxygen-deficient and oxygen-rich water on the degradation of pollutants

The reaction pathway of organic pollutants degraded with Fe NPs can be divided into two types: indirect oxidation and direct reduction. Indirect oxidation is a heterogeneous Fenton reaction for advanced oxidation degradation of organic pollutants by Fe NP, just as it is a high-level process under the condition of dissolved oxygen while the direct reduction takes place in the absence of oxygen in which Fe NP acts as a reducing agent and loses electrons to the contaminants, so that toxic pollutants may be converted into non-toxic or less toxic substances. To understand whether the mechanism of degradation of 4-NP by Fe NP belongs to indirect oxidation or direct reduction, we simulated oxygen-enriched water and oxygen-deficient water by exposing the mixture to air and argon gas, respectively.

2.7. Effects of coexisting different metal ions

When another metal with a higher reduction potential is added to the surface of the Fe NPs, a bimetallic system is made. This makes the nano-iron work better. To explore this phenomenon, we measured the degradation rates in the presence of different metal ions at a concentration of 3 mmol/L.

3. Results and discussion

3.1. X-ray diffraction

It can be observed from Fig. 1 that the prepared samples produce a strong diffraction peak at 44.67°. As can be seen from the JCPDF (06-0696) standard card, this characteristic peak belongs to the diffraction peak of the Fe element, so the Fe NP sample with high purity and crystallinity was successfully prepared by liquid phase reduction.

3.2. X-ray photoelectron spectroscopy

Analysis of different elements in Fe NP by XPS shows no impurity peaks for other elements except for C, O, and Fe. In XPS survey spectra, carbon remains intact, but oxygen is only present because it is present as an oxide coating on the outermost layer of the iron nanoparticles. A small peak at about 56.08 eV can be observed from Fig. 2a which belongs to the binding energy peak of Fe $2p_{3/2}$. From the

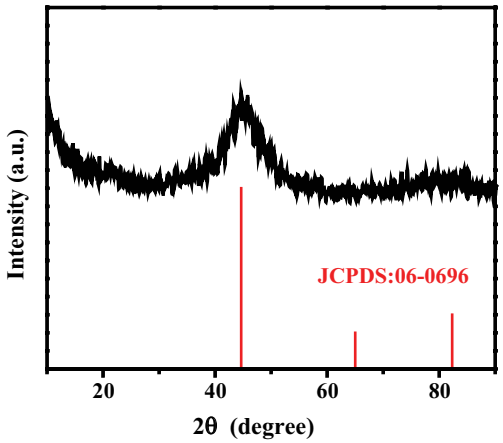

Fig. 1. X-ray diffraction atlas of the Fe nanoparticle sample.

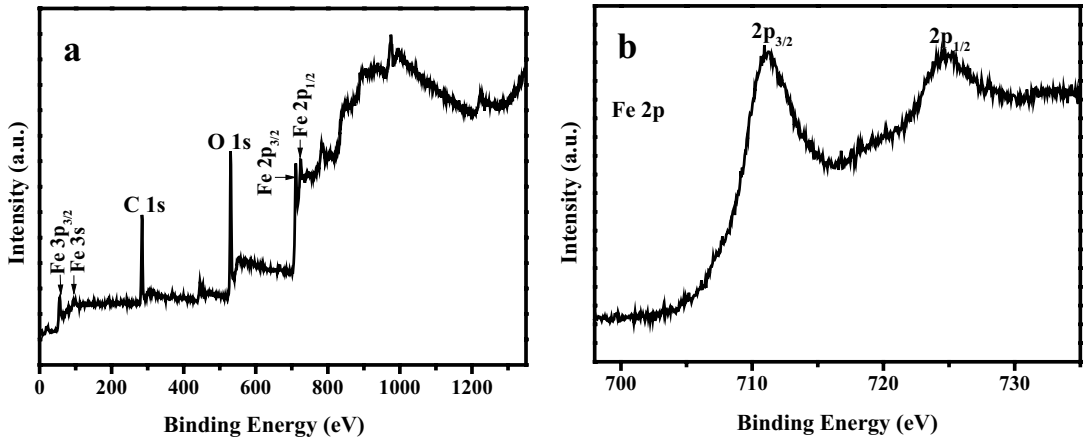

Fig. 2. Full X-ray photoelectron spectrum of Fe NP sample (a), high-resolution X-ray photoelectron spectra of elemental Fe (b).

high-resolution XPS spectra in Fig. 2b, it can be observed that the $2p_{3/2}$ and $2p_{1/2}$ binding energies of Fe are located at about 710.9 and 725.63 eV, respectively indicating that the valence state of iron in Fe NP is zero which further confirms that the prepared sample is zero-valent iron nanoparticles.

3.3. Morphology

The SEM image of the freshly prepared Fe NP sample by liquid phase reduction method is shown in Fig. 3. From Fig. 3a and b, it can be observed that the freshly prepared Fe NPs are spherical. It is found that the particles have different degrees of adhesion. The freshly prepared Fe NPs are agglomerated in a chain-like manner, and their average diameter is 25–150 nm. From the transmission electron microscopy image in Fig. 3c and d, it can be observed that the surface of Fe NP is smooth and spherical, and the particles are agglomerated in a chain-like manner with less uniform size and an average particle size of about 30–230 nm.

3.4. Standard curve and maximum absorption wavelength analysis

Drawing of the standard curve: eight volumetric flasks each of 100 mL volume were taken, solution of different concentrations (1, 3, 5, 7.5, 8.75, 10, 15, and 20 mg/L) were prepared, using deionized water as a solvent under shaking. Using distilled water as a reference, the absorbance of the 4-NP solution at a maximum absorption wavelength of 317 nm was determined by a dual-beam UV-Vis spectrophotometer model TU-1901. Determination of maximum absorption wavelength: 100 mg nano-zero-valent iron degradation concentration of 15 mg/L and volume of 200 mL p-nitrophenol solution were taken and after every 0, 5, 10, 20, 40, and 60 min, their absorbances were measured in the wavelength range of 250–350 nm. From the data presented in Fig. 4a, the absorbance and concentration of the 4-NP solution in the range of 1~20 mg/L are well linearly fitted to obey the equation of the straight line ($y = 0.06796x - 0.00128$) with a correlation coefficient (R^2) of 0.9991. Fig. 4b shows the maximum absorption wavelength change analysis during the degradation experiment. The absorbance curves after 60 min are not changed much and are actually highly coincident with each other, so they are not shown. With the extension of degradation time, the intensity of the peak gradually decreased, indicating that the nitro group on p-nitrophenol is effectively reduced during the reaction catalyzed by Fe NPs. And during the degradation of 4-NP in the presence of a catalyst of Fe NPs, the absorbance of 4-NP produces a blue shift phenomenon, that is, its maximum absorption wavelength of 317 nm before the catalytic degradation changes to 297 nm after the degradation starts for about 10 min. The reason for this may be that 4-NP will form intermediates first during the degradation process after at least 5 min, therefore the blue shift is not significant until the number of intermediates produced is dominant after about 10 min. As the time of reaction increases, the more intermediate products accumulate, the more pronounced the shift of the maximum absorption peak to the lower wavelengths.

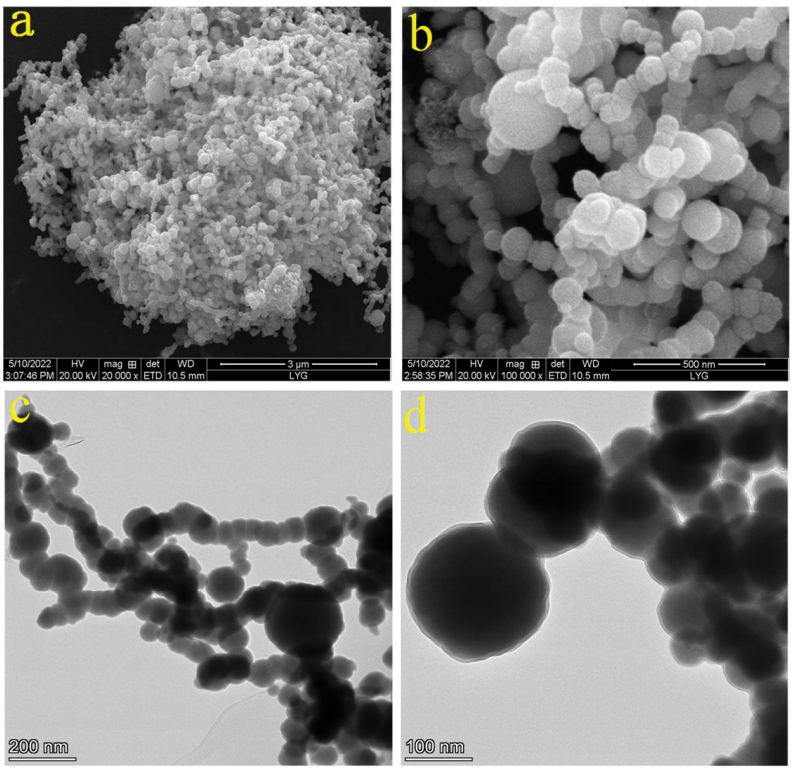

Fig. 3. Scanning electron microscopy images (a,b) and high-resolution transmission electron microscopy images (c,d) of the prepared Fe NPs.

3.5. Degradation

The experimental data in Fig. 5a shows the self-degradation of 4-NP. It can be seen that the absorbance of 4-NP in 4 h is about 1.010 indicating that 4-NP is extremely stable in the water environment and is not easy to self-degrade. From the data, it can be seen that the degradation of 4-NP in the presence of Fe NPs is completely reactive after 60 min. The experimental data in Fig. 5b shows the degradation of 4-NP in the presence of 50 mg nano-iron and the blank control

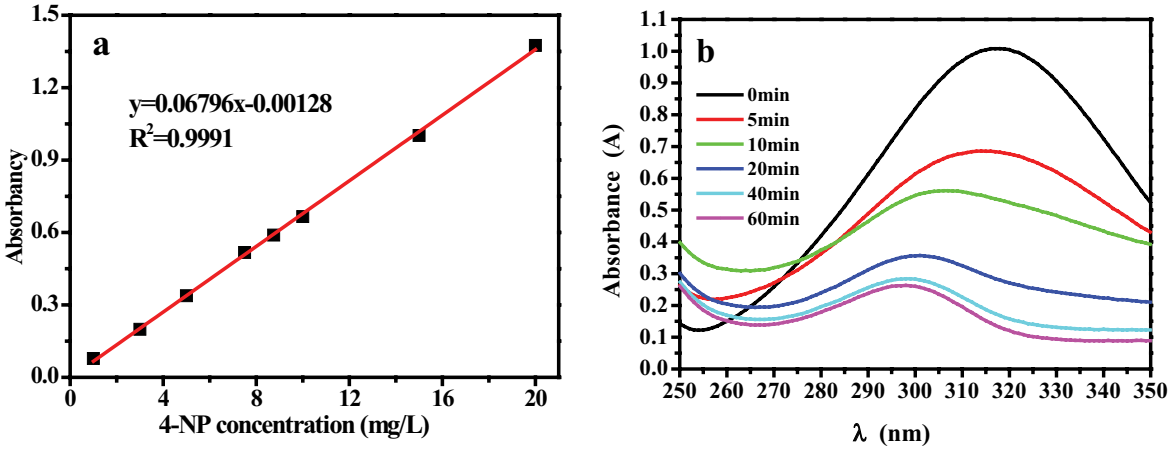

Fig. 4. p-nitrophenol standard curve (a) and diagram of the maximum absorption wavelength change of Fe NPs catalyzed degradation of p-nitrophenol (b).

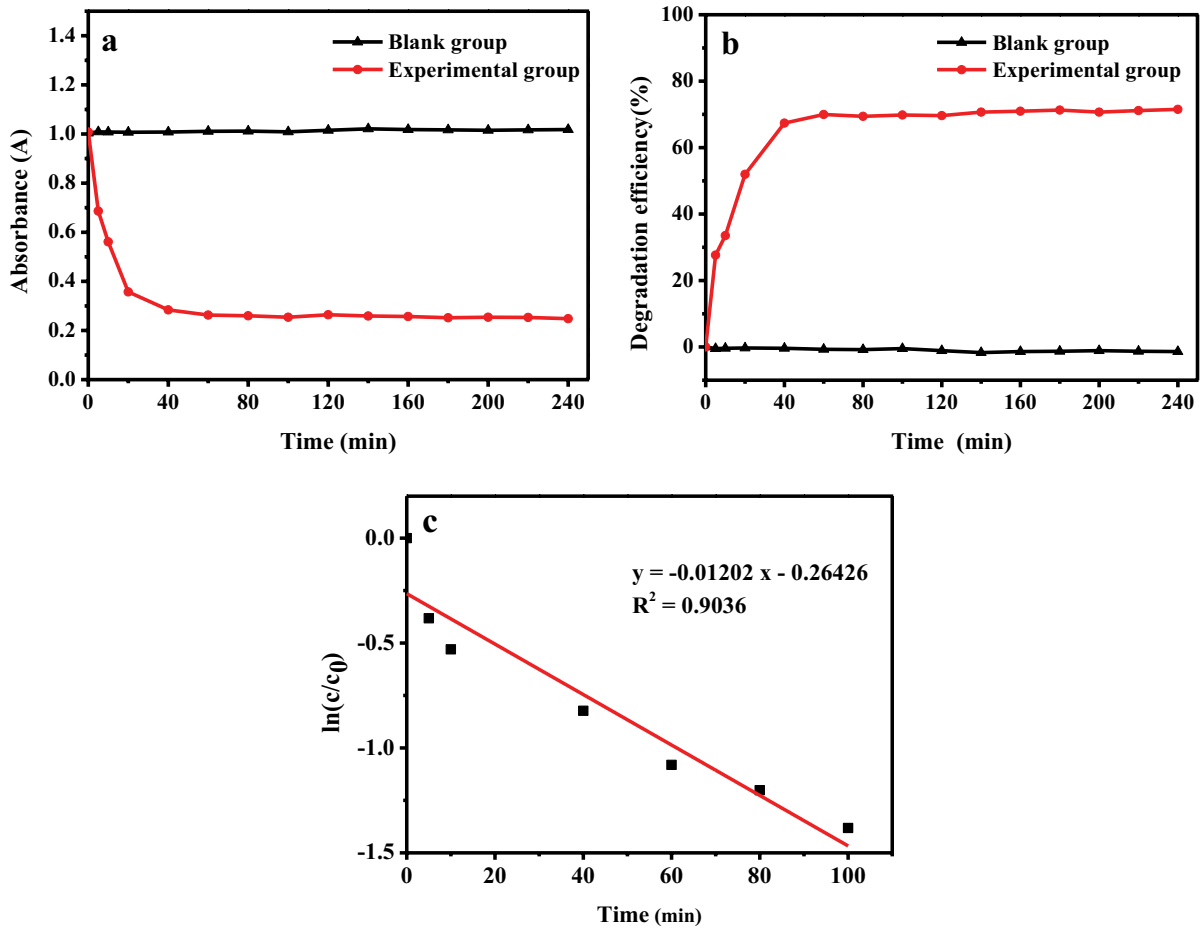

Fig. 5. The self-degradation chart of p-nitrophenol (a), catalytic degradation of p-nitrophenol by Fe NPs (b), reaction rate plot of Fe NP degrades p-nitrophenol (c).

is 4-NP solution without adding Fe NPs. Again, it can be seen that the self-degradation rate of 4-NP is close to zero within 4 h indicating that 4-NP does not undergo self-degradation under the experimental condition, and the degradation rate tends to be stable after 60 min, so it can be considered that the reaction has been complete in this period. The iron nanoparticles degrade 74% of 15 mg/L p-nitrophenol within 60 min, compared with literature [47,48], it has a higher degradation rate. This material has great prospects in degrading organic pollution.

The degradation rates of p-nitrophenol in 5, 10, 20, 40, 60, 80, and 100 min are 32%, 44%, 65%, 72%, 74%, 74%, and 75%, respectively. The degradation of 4-NP with Fe NPs is a solid–liquid interphase reaction. Therefore, the experimental data can be fitted using a first-order reaction model; $\ln(c/a) = kt$, where c and a (mg/L) are the concentrations of the residual 4-NP solution in the system and the initial concentration of the 4-NP solution before the catalytic degradation in the presence of Fe NPs carried out for time t, and k is the rate constant. $\ln(c/a)$ has a linear relationship with t. When $\ln(c/a)$ is plotted on the y-axis and time t on the x-axis, the slope shows the rate constant. It can be seen from Fig. 5c that the experimental data can be well fitted to the first-order reaction model, with a correlation R^2 of 0.9036, and rate constant k of – 0.01202.

3.6. Degradation effect analysis of 4-NP under different conditions

Fig. 6a shows that the degradation rate and the final degradation of 4-NP are much better in oxygen-poor water. This suggests that the mechanism direct reduction is involved in the 4-NP breaking with Fe NP rather than indirect oxidation.

From Fig. 6b, it is understandable that the activity of Fe NP increases in the presence of Cu^{2+} ions while other three metals significantly reduce the activity of iron nanoparticles. The reason is that one of the conditions that constitute the battery is that there are two electrodes with different activities. Manganese, zinc, and iron are all active metals, so zinc and manganese are difficult to form electrochemical micro batteries on the surface of nano-iron, which hinder the transfer of electrons, thereby reducing the activity of iron nanoparticles to degrade 4-NP. In contrast, when Cu^{2+} is added to the system, Fe NP reduces Cu^{2+} ions to elemental copper thereby forming an electrochemical microcell on the surface of the Fe NP which promotes electron transfer and improves the activity of Fe NP for the degradation of 4-NP.

As shown in Fig. 6c, when the doped Cu^{2+} concentration is 3 mmol/L, the degradation rate of 4-NP by Fe NP is the highest, and the degradation of 4-NP in 4 h reaches 83.55%. When the Cu^{2+} concentration is too low or too high,

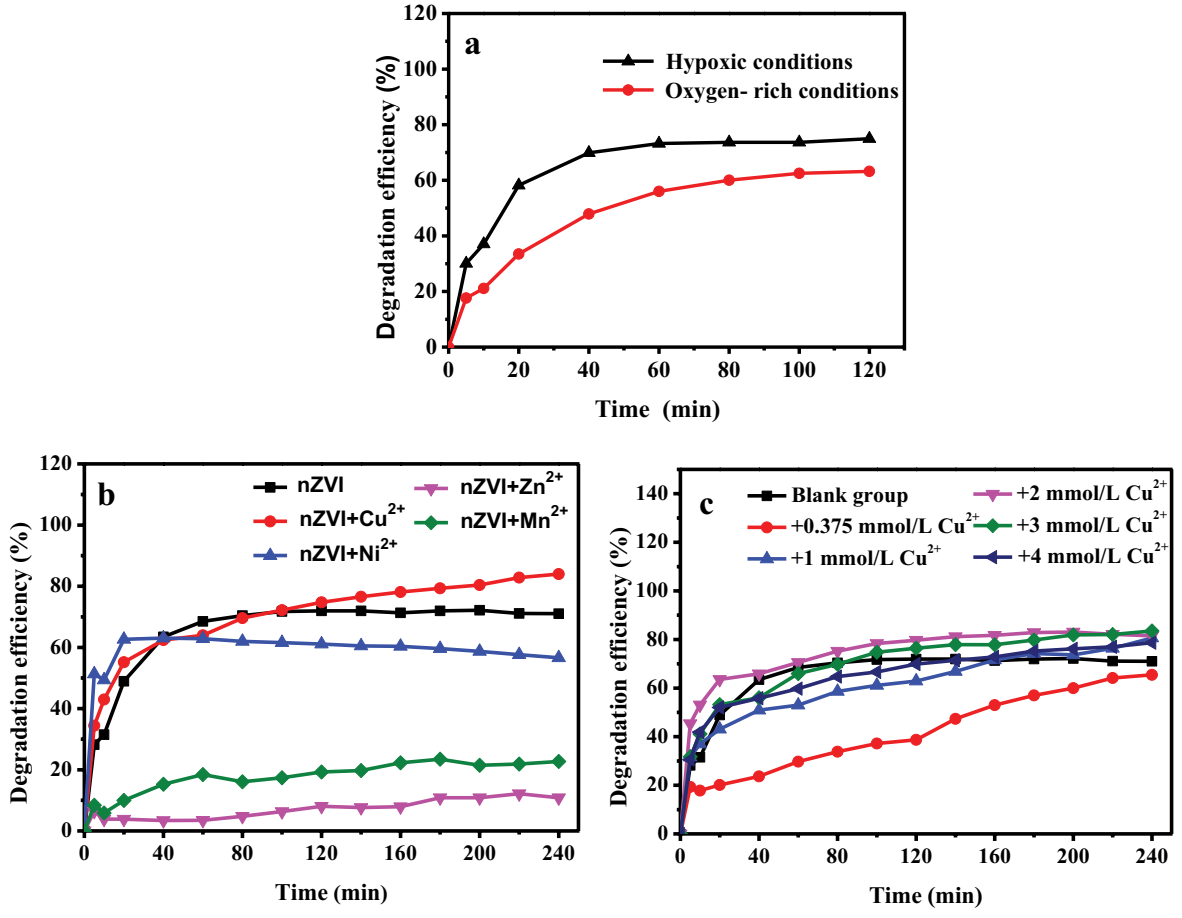

Fig. 6. Degradation rate of p-nitrophenol over Fe NP under hypoxic and oxygen-rich conditions (a), in the presence of different metal ions (b), and at different concentrations of copper ions (c).

the degradation rate is lower. The reason may be when the Cu^{2+} concentration is too low, the reduction of copper ions by Fe NP is too low to form a micro-battery on the surface of most Fe NPs. This weakens the electron transfer and reduces the activity of Fe NP to degrade 4-NP. When the Cu^{2+} concentration is too high, too much Fe NP is consumed resulting in a decrease in the amount of catalyst to slow down the degradation process.

3.7. Mechanism of Fe NP catalytic reduction of 4-NP

In recent years, the abuse and discharge of organic pollutants have posed a serious threat to the organisms and environment. p-nitrophenol, also known as 4-nitrophenol, is an organic compound with the chemical formula $C_6H_5NO_3$. It is a colorless to yellowish crystalline powder, soluble in hot water, ethanol, ether, and chloroform, and mainly used as an intermediate for fine chemicals such as pesticides, pharmaceuticals, dyes, etc. Because of its high stability and difficult biodegradation, researchers have paid extensive attention to finding efficient ways to remove 4-NP from water. To resolve the pollution caused by 4-NP in the water environment effectively, many chemical methods for degrading antibiotics, such as external current and strong oxidants, began to appear in the eyes of people, among which the room temperature catalysis technology has been widely explored and used as an efficient, low-cost, and environment-friendly organic sewage treatment method. To make full use of catalysts effectively for degrading 4-NP in water, it is urgent to develop new materials with high catalytic activity that can be applied in aqueous solutions.

In this work, although argon gas discharges part of the oxygen, it belongs to the hypoxic state, but there is still oxygen in the solution, Fe NP has strong reducibility, by reducing dissolved oxygen in the aqueous solution to hydrogen peroxide that can produce hydroxyl radicals, organic pollutants can be degraded. For acidic 4-NP solution, the following two possible mechanisms are proposed based on experimental results. First, through double electron transport in more acidic solutions, dissolved oxygen can be reduced to hydrogen peroxide (H_2O_2) by Fe NPs, and the resulting H_2O_2 can be reduced to water by Fe NPs. Catalyzed by Fe^{2+}, H_2O_2 produces strongly reactive oxidizing substances such as hydroxyl radicals ($^{\bullet}OH$). It can effectively catalyze the degradation of organic contaminant 4-NP [49]. In addition, elemental iron can also generate iron hydroxides in water, which have a flocculating effect on pollutants, can adsorb some pollutants, and achieve the purpose of degrading 4-NP pollutants.

$$Fe^{o} + O_2 + 2H^{+} \rightarrow Fe^{2+} + H_2O_2 \quad (1)$$

$$Fe^{o} + H_2O_2 + 2H^{+} \rightarrow Fe^{2+} + 2H_2O \quad (2)$$

$$Fe^{2+} + H_2O_2 \rightarrow Fe^{3+} + {}^{\bullet}OH + OH^{-} \quad (3)$$

4. Conclusion

In this work, Fe NPs with high purity and crystallinity were successfully prepared by the liquid phase reduction method. Through experimentation, it was found that the absorbance and concentration of 4-NP solution in the range of 1~20 mg/L were well linearly fitted, and the correlation coefficient was $R^2 = 0.9991$. The catalytic degradation results showed that 4-NP did not degrade itself, and when Fe NP was added, the degradation of 4-NP reached completion in 60 min with a degradation efficiency of 74%. In addition, this experiment also explored the degradation rate of 4-NP in different water bodies, in the presence of different interfering ions at different concentrations and concluded that when the environment was hypoxic and the doped Cu^{2+} concentration was 3 mmol/L, the degradation efficiency of Fe NPs for 4-NP was the highest, reaching about 84%.

Acknowledgments

This work was financially supported by National Natural Science Foundation of China (Grants 52272287 and 22268003) and the Science and Technology Project of Yunnan (202305AF150116, 202301AT070027 and 230212526080).

Notes

The authors declare no competing financial interests.

References

[1] L.X. Li, J.P. Zhang, A.Q, Wang, Removal of organic pollutants from water using superwetting materials, Chem. Rec., 18 (2018) 118–136.
[2] K.Z. Qi, C.Q. Zhuang, M.J. Zhang, P. Gholami, A. Khataee, Sonochemical synthesis of photocatalysts and their applications, J. Mater. Sci. Technol., 123 (2022) 243–256.
[3] X. He, J.M. Xia, J.L. He, K.Z. Qi, A.Z. Peng, Y. Liu, Highly efficient capture of heavy metal ions on amine-functionalized porous polymer gels, Gels, 9 (2023) 297, doi: 10.3390/gels9040297.
[4] J.J. Zhang, A. Bifulco, P. Amato, C. Imparato, K.Z. Qi, Copper indium sulfide quantum dots in photocatalysis, J. Colloid Interface Sci., 638 (2023) 193–219.
[5] Q.F. Cui, X.Y. Gu, Y. Zhao, K.Z. Qi, Y. Yan, S-scheme $CuInS_2$/ZnS heterojunctions for the visible light-driven photocatalytic degradation of tetracycline antibiotic drugs, J. Taiwan Inst. Chem. Eng., 142 (2023) 104679, doi: 10.1016/j.jtice.2023.104679.
[6] I. Khan, M. Luo, L. Guo, S. Khan, C.J. Wang, A. Khan, M. Saeed, S. Zaman, K.Z. Qi, Q.L. Liu, Enhanced visible-light photoactivities of porous $LaFeO_3$ by synchronously doping Ni^{2+} and coupling TS-1 for CO_2 reduction and 2,4,6-trinitrophenol degradation, Catal. Sci. Technol., 11 (2021) 6793–6803.
[7] C. Liu, Z. Qiang, C. Adams, F. Tian, T. Zhang, Kinetics and mechanism for degradation of dichlorvos by permanganate in drinking water treatment, Water Res., 43 (2009) 3435–3442.
[8] X.Y. Liao, D. Zhao, X.L. Yan, Determination of potassium permanganate demand variation with depth for oxidation-remediation of soils from a PAHs-contaminated coking plant, J. Hazard. Mater., 193 (2011) 164–170.
[9] F.S. Ali, K.Z. Qi, B. Al Wahaibi, M.A. Meetani, H. Al Lawati, Y.H. Lim, S.M.Z. Al Kindy, R. Selvaraj. Photocatalytic degradation of Bisphenol A in the presence of TiO_2 nanoparticle: effect of solvent on size control, Desal. Water Treat., 79 (2017) 301–307.
[10] W.C. Yang, Y.J. Zhang, J.H. Zheng, L. Liu, M.Y. Si, Q. Liao, Z.H. Yang, F.P. Zhao, Migration of spent grain-modified colloidal ferrihydrite: implications for the *in-situ* stabilization of arsenic, lead, and cadmium in co-contaminated soil, Chemosphere, 344 (2023) 140310, doi: 10.1016/j.chemosphere.2023.140310.
[11] L. Liu, Z.H. Yang, W.C. Yang, W. Jiang, Q. Liao, M.Y. Si, F.P. Zhao, Ferrihydrite transformation impacted by coprecipitation of lignin: inhibition or facilitation?, J. Environ. Sci., 139 (2024) 23–33.

[12] L. Liu, Z.H. Yang, F.P. Zhao, Z.T. Chai, W.C. Yang, H.R. Xiang, Q. Liao, M.Y. Si, Z. Lin, Manganese doping of hematite enhancing oxidation and bidentate-binuclear complexation during As(III) remediation: experiments and DFT calculation, Chem. Eng. J., 471 (2023) 144758, doi: 10.1016/j.cej.2023.144758.
[13] H. Liu, Y.X. Fu, S.X. Chen, W.C. Zhang, K.S. Xiang, F.H. Shen, R.Y. Xiao, L.Y. Chai, F.P. Zhao, A layered g-C_3N_4 support Single-Atom Fe-N_4 catalyst derived from hemin to activate PMS for selective degradation of electron-rich compounds via singlet oxygen species, Chem. Eng. J., 474 (2023) 145571, doi: 10.1016/j.cej.2023.145571.
[14] H.R. Xiang, Z.H. Yang, S.Z. Liu, X.Q. Li, C.Y. Yang, Y. Ke, X.Y. Liu, F.P. Zhao, M.Q. Shi, Z. Lin, Natural pyrite-assisted mechanochemical recovery of insoluble manganese from electrolytic manganese residue: kinetics and mechanisms, ACS EST Eng., 3 (2023) 1661–1673.
[15] N. Cui, A. Zada, J.H. Song, Y.Z. Yang, M.H. Liu, Y. Wang, Y.X. Wu, K.Z. Qi, R.S. Selvaraj, S-Y. Liu, G. Jin, Plasmon-induced ZnO-Ag/AgCl photocatalyst for degradation of tetracycline hydrochloride, Desal. Water Treat., 245 (2022) 247–257.
[16] K.Z. Qi, S-Y. Liu, R. Selvaraj, W. Wang, Z.X. Yan, Comparison of Pt and Ag as co-catalyst on g-C_3N_4 for improving photocatalytic activity: experimental and DFT studies, Desal. Water Treat., 153 (2019) 244–252.
[17] J.J. Zhang, Y. Zhao, K.Z. Qi, S.Y. Liu, $CuInS_2$ quantum-dot-modified g-C_3N_4 S-scheme heterojunction photocatalyst for hydrogen production and tetracycline degradation, J. Mater. Sci. Technol., 172 (2024) 145–155.
[18] J.J. Zhang, Y. Zhao, K. Zhang, A. Zada, K.Z. Qi, Sonocatalytic degradation of tetracycline hydrochloride with $CoFe_2O_4$/g-C_3N_4 composite, Ultrason. Sonochem., 94 (2023) 106325, doi: 10.1016/j.ultsonch.2023.106325.
[19] S. Afzal, N.M. Julkapli, L.K. Mun, Response surface approach for visible light assisted photocatalytic degradation of ortho nitrophenol by magnetically separable TiO_2/CS nanocomposite, Mater. Sci. Semicond. Process., 99 (2019) 34–43.
[20] Y. Zhao, P. Yuan, X. Xu, J.Y. Yang, Removal of p-nitrophenol by adsorption with 2-phenylimidazole-modified ZIF-8, Molecules, 28 (2023) 4195, doi: 10.3390/molecules28104195.
[21] M. Khatamian, A.A. Khandar, B. Divband, M. Haghighi, S. Ebrahimiasl, Heterogeneous photocatalytic degradation of 4-nitrophenol in aqueous suspension by Ln (La^{3+}, Nd^{3+} or Sm^{3+}) doped ZnO nanoparticles, J. Mol. Catal. A: Chem., 365 (2012) 120–127.
[22] M.S.S. Ezzuldin, S.N.A. Md. Jamil, L.C. Abdullah, T.S.Y. Choong, T.M. Ting, Insights into the p-nitrophenol adsorption by amidoxime-modified poly(acrylonitrile-co-acrylic acid): characterization, kinetics, isotherm, thermodynamic, regeneration and mechanism study, RSC Adv., 11 (2021) 8150–8162.
[23] S. Rawat, J. Singh, J.R. Koduru, Effect of ultrasonic waves on degradation of phenol and para-nitrophenol by iron nanoparticles synthesized from Jatropha leaf extract, Environ. Technol. Innovation, 24 (2021) 101857, doi: 10.1016/j.eti.2021.101857.
[24] Y.X. Wang, X.J. Ye, G.B. Chen, D.Z. Li, S.G. Meng, S.F. Chen, Synthesis of $BiPO_4$ by crystallization and hydroxylation with boosted photocatalytic removal of organic pollutants in air and water, J. Hazard. Mater., 399 (2020) 122999, doi: 10.1016/j.jhazmat.2020.122999.
[25] Y. Yue, Y.X. Wang, C. Qu, X.D. Xu, Modification of polyacrylonitrile-based activated carbon fibers and their p-nitrophenol adsorption and degradation properties, J. Environ. Chem. Eng., 9 (2021) 105390, doi: 10.1016/j.jece.2021.105390.
[26] J. Lee, J.C. Park, H.A. Song, Nanoreactor framework of a Au@SiO_2 yolk/shell structure for catalytic reduction of p-nitrophenol, Adv. Mater., 20 (2008) 1523–1528.
[27] J.G. Mahy, L. Tasseroul, A. Zubiaur, J. Geens, M. Brisbois, M. Herlitschke, R. Hermann, B. Heinrichs, S.D. Lambert, Highly dispersed iron xerogel catalysts for p-nitrophenol degradation by photo-Fenton effects, Microporous Mesoporous Mater., 197 (2014) 164–173.
[28] Z.D. Pozun, S.E. Rodenbusch, E. Keller, K. Tran, W.J. Tang, K.J. Stevenson, G. Henkelman, A systematic investigation of p-nitrophenol reduction by bimetallic dendrimer encapsulated nanoparticles, J. Phys. Chem. C, 117 (2013) 7598–7604.
[29] L. Zhou, M. Zhou, Z. Hu, Z.H. Bi, K.G. Serrano, Chemically modified graphite felt as an efficient cathode in electro-Fenton for p-nitrophenol degradation, Electrochimic. Acta, 140 (2014) 376–383.
[30] C. Li, P. Wang, Y. Tian, X.L. Xu, H. Hou, M.M. Wang, G.H. Qi, Y.D. Jin, Long-range plasmon field and plasmoelectric effect on catalysis revealed by shell-thickness-tunable pinhole-free Au@SiO_2 core–shell nanoparticles: a case study of p-nitrophenol reduction, ACS Catal., 7 (2017) 5391–5398.
[31] V.V. Kadam, S.D. Shanmugam, J.P. Ettiyappan, R.M. Balakrishnan, Photocatalytic degradation of p-nitrophenol using biologically synthesized ZnO nanoparticles, Environ. Sci. Pollut. Res. Int., 28 (2021) 12119–12130.
[32] S. Galyaltdinov, A. Svalova, V. Brusko, M. Kirsanova, A.M. Dimiev, Nickel on oxidatively modified carbon as a promising cost-efficient catalyst for reduction of p-nitrophenol, Molecules, 27 (2022) 5637, doi: 10.3390/molecules27175637.
[33] C. Karthikeyan, M. Ranjani, A.R. Kim, D.J. Yoo, G.G. Kumar, Synthesis of iron nanoparticles using *Azadirachta indica* extract and its catalytic activity toward nitrophenol reduction, J. Nanosci. Nanotechnol., 16 (2016) 2527–2533.
[34] A. Leovac Macerak, A. Kulic Mandic, V. Pesic, D. Tomasevic Pilipovic, M. Becelic-Tomin, D. Kerkez, "Green" nZVI-biochar as Fenton catalyst: perspective of closing-the-loop in wastewater treatment, Molecules, 28 (2023) 1425, doi: 10.3390/molecules28031425.
[35] G. Cagnetta, J. Huang, I.O. Lomovskiy, G. Yu, Tailoring the properties of a zero-valent iron-based composite by mechanochemistry for nitrophenols degradation in wastewaters, Environ. Technol., 38 (2017) 2916–2927.
[36] J. Fan, Y. Guo, J. Wang, M.H. Fan, Rapid decolorization of azo dye methyl orange in aqueous solution by nanoscale zerovalent iron particles, J. Hazard. Mater., 166 (2009) 904–910.
[37] S.R. Kanel, B. Manning, L. Charlet, H. Choi, Removal of arsenic(III) from groundwater by nanoscale zero-valent iron, Environ. Sci. Technol., 39 (2005) 1291–1298.
[38] W. Yan, A.A. Herzing, C.J. Kiely, W.X. Zhang, Nanoscale zero-valent iron (nZVI): aspects of the core-shell structure and reactions with inorganic species in water, J. Contam. Hydrol., 118 (2010) 96–104.
[39] X.Q. Li, J.S. Cao, W.X. Zhang, Stoichiometry of Cr(VI) immobilization using nanoscale zerovalent iron (nZVI): a study with high-resolution X-ray photoelectron spectroscopy (HR-XPS), Ind. Eng. Chem. Res., 47 (2008) 2131–2139.
[40] M.N. Nadagouda, A.B. Castle, R.C. Murdock, S.M. Hussain, R.S. Varma, *In-vitro* biocompatibility of nanoscale zerovalent iron particles (NZVI) synthesized using tea polyphenols, Green Chem., 12 (2010) 114–122.
[41] Q. Wang, S.R. Kanel, H. Park, A. Ryu, H. Choi, Controllable synthesis, characterization, and magnetic properties of nanoscale zerovalent iron with specific high Brunauer–Emmett–Teller surface area, J. Nanopart. Res., 11 (2008) 749–755.
[42] W. Wang, Z.H. Jin, T.L. Li, H. Zhang, S. Gao, Preparation of spherical iron nanoclusters in ethanol-water solution for nitrate removal, Chemosphere, 65 (2006) 1396–1404.
[43] J.F. Liu, X.Z. Zheng, L.L. Pan, X.L. Fu, X.J. Zhang, S.G. Meng, S.F. Chen, Efficient photocatalytic H_2 production coupling with selective oxidation of aromatic alcohol under carbon neutrality, Appl. Catal., B, 298 (2021) 120619, doi: 10.1016/j.apcatb.2021.120619.
[44] F. Zhu, L. Li, W. Ren, X.Q. Deng, T. Liu, Effect of pH, temperature, humic acid and coexisting anions on reduction of Cr(VI) in the soil leachate by nZVI/Ni bimetal material, Environ. Pollut., 227 (2017) 444–450.
[45] E.J. Kim, K. Murugesan, J.H. Kim, P.G. Tratnyek, Y.S. Chang, Remediation of trichloroethylene by FeS-coated iron nanoparticles in simulated and real groundwater: effects of water chemistry, Ind. Eng. Chem. Res., 52 (2013) 9343–9350.

[46] S. Dutta, R. Saha, H. Kalita, A.N. Bezbaruah, Rapid reductive degradation of azo and anthraquinone dyes by nanoscale zero-valent iron, Environ. Technol. Innovation, 5 (2016) 176–187.
[47] S. Chahal, L. Phor, S. Singh, A. Singh, J. Malik, P. Goel, A. Kumar, S. Kumar, Ankita, P. Kumar, An efficient and unique method for the growth of spindle shaped Mg-doped cerium oxide nanorods for photodegradation of p-nitrophenol, Ceram. Int., 48 (2022) 28961–28968.
[48] X. Liu, L.H. Zhao, H. Lai, X. Zhang, Z.J. Yi, Highly effective degradation of p-nitrophenol over MoS_2 under visible light illumination, Catal. Lett., 147 (2017) 2153–2159.
[49] X.Z. Zheng, Z. Zhang, S.G. Meng, Y.X. Wang, D.Z. Li, Regulating charge transfer over 3D Au/ZnO hybrid inverse opal toward efficiently photocatalytic degradation of bisphenol A and photoelectrochemical water splitting, Chem. Eng. J., 393 (2020) 124676, doi: 10.1016/j.cej.2020.124676.